Carbohydrate Polymers 83 (2011) 1245–1252

Contents lists available at ScienceDirect

Carbohydrate Polymers

journal homepage: www.elsevier.com/locate/carbpol

Effect of sonication and aging on the templating attribute of starch for "green" silver nanoparticles and their interactions at bio-interface

Rocktotpal Konwarh[a], Niranjan Karak[a,*], Clara Ermine Sawian[b], Shashi Baruah[b], Manabendra Mandal[b]

[a] Advanced Polymer and Nanomaterial Laboratory, Department of Chemical Sciences, Tezpur University, Sonitpur 784028, Assam, India
[b] Department of Molecular Biology and Biotechnology, Tezpur University, Sonitpur 784028, Assam, India

ARTICLE INFO

Article history:
Received 14 July 2010
Received in revised form
14 September 2010
Accepted 16 September 2010
Available online 24 September 2010

Keywords:
Starch template
Silver nanoparticles
Sonication
Response surface methodology
Phytotoxicity
Anti-microbial

ABSTRACT

The present work reports the exploitation of starch as a macromolecular matrix in the domain of 'green' bio-nanotechnology. The differential templating attributes of starch under ambient aging and sonication for biomimetically generated silver nanoparticles were investigated. Morphology-directing action of the starch-bioreductant (i.e., *Mesua ferrea* Linn. leaf aqueous extract, adjusted to basic pH) complex resulted in a branched silver structure (~440 nm, along the long axis with branch average diameter of 11.5 nm) upon aging for 24 days. Starch assisted spherical silver nanoparticles (average diameter, 5.4 nm) were obtained under sonication parameters of 3 min, 0.5 cycles at 60% amplitude, optimized through response surface methodology. Evaluation of phytotoxicity on *Cucumis sativus*, compromise on amplification of a 263 base pair mammalian DNA sequence in polymerase chain reaction (PCR) and anti-microbial potency demonstrated differential action of the carbohydrate templated aged and sonicated silver nanoparticles at the bio-interface.

© 2010 Elsevier Ltd. All rights reserved.

1. Introduction

The novel properties of nanoparticles, primarily attributed to the quantum size effect are confronted by their conventional ecologically hazardous synthesis protocols (Jackson & Halas, 2001). Endeavors are underway to develop greener avenues in the domain of nanotechnology. In this context, Sharma, Yngard, and Lin (2009), Korbekandi, Iravani, and Abbasi (2009) have reviewed the various green strategies using myriad of bioresources explored for the preparation of nanoparticles. It is pertinent to mention that carbohydrate templated silver nanoparticles (Babu, Kim, Kim, Ahn, & Lee, 2010) have carved a unique niche in the domain of nanobiotechnology with an immense spectrum of applications particularly as anti-microbial bio-polymer nanocomposite. Macromolecules, such as starch, when used for encapsulation or entrapment of inorganic particles can impart novel properties to the latter (Ziolo et al., 1992). Enhanced compatibility, reduced leaching and protection of the surfaces from damage with concomitant improvement in dispersibility and stability of the nanoparticles are few of the desired facets of polymer templated nanomaterial over the uncoated counterparts (Bourgeat-Lami & Lang, 1998).

We have recently reported the exploitation of *Mesua ferrea* L. aqueous leaf extract as reducing agent, adjusted to basic pH for the preparation of poly(ethylene glycol) (PEG) supported silver nanoparticles (Konwarh, Kalita, Mahanta, Mandal, & Karak, 2010). The leaf components (Govindachari, Viswanathan, Pai, Rao, & Srinivasan, 1967) including triedelin and triterpenes of the friedelin group, namely canophyllal, canophyllol and canophyllic acid are envisaged as active components for the generation of the nanoparticles.

The templating attribute of starch in lieu of the previously reported polymer, i.e., PEG (Konwarh et al., 2010) is reported in this work. The right-handed helical conformation of starch in aqueous solution, with extensive number of hydroxyl groups can facilitate the complexation of metal ions to the molecular matrix. The green capping and stabilizing attribute (Bozanic et al., 2007; Singh, Sinha, & Mandal, 2009; Singh, Sinha, Singh, & Mandal, 2010), morphology-directing action (Vigneshwaran, Nachane, Balasubramanya, & Varadarajan, 2006) and effective reductive potency of starch (Lu, Gao, & Komarneni, 2005) under microwave-assistance or hydrothermal energy for generation of nanoparticles have already been exploited. In the present system, we report the use of starch as templating matrix and the reductive potential of *M. ferrea* L. leaf aqueous extract for the preparation of silver nanoparticles at ambient temperature, eliminating the additional energy input. We have tried to explore the effects of aging and sonication on the generation of silver nanoparticles. The cavita-

* Corresponding author. Tel.: +91 3712 267009; fax: +91 3712 267006.
E-mail address: karakniranjan@yahoo.com (N. Karak).

0144-8617/$ – see front matter © 2010 Elsevier Ltd. All rights reserved.
doi:10.1016/j.carbpol.2010.09.031

tion forces induced during transient collapse of cavitating bubbles are of immense significance, particularly in the domain of material science. Statistical optimization of the various sonication parameters has been devised to obtain narrow-sized silver nanoparticles, as indicated by λ_{max} position in the UV–vis spectra.

Preparation of nanoparticles through 'green' routes also demands adequate eco-toxicological testing and establishment of biocompatibility before their commercialization, particularly for biomedical-niche applications. Limited phytotoxicity studies have reported both positive and negative effects of nanoparticles on higher plants. Seed germination and root elongation is a rapid and widely used acute phytotoxicity test with several advantages: sensitivity, simplicity, low cost and suitability for unstable chemicals or samples (Lin & Xing, 2008; Yang et al., 2006). It is expected that starch (a bio-polymer that is commercially extracted from plant sources) templated nanomaterial should be biocompatible with plant species. However, this may not be the case always. In order to evaluate this, we had tried to assess the phytotoxicity of the prepared samples (the unsonicated/aged and the sonicated) on *Cucumis sativus* (cucumber), a plant among the 10 recommended species by USEPA (1966) for the determination of ecological effects of pesticides and toxic substances.

Polymerase chain reaction (PCR) is used to amplify a single or few copies of a piece of DNA across several orders of magnitude, generating a library of copies of the particular DNA sequence. Compromise with the replication fidelity of DNA in PCR is a recently reported tool to assess preliminary genotoxicity of nanoparticles. It has been reported that silver nanoparticles of food storage material interfere with DNA replication fidelity and bind with DNA, visualized through atomic force microscopy (Yang et al., 2009). In our experiment, we employed a mammalian 263 base pair target sequence in order to assess the potential toxicity of the prepared samples. Furthermore, the starch templated silver nanoparticles were assessed for their anti-microbial potency.

Thus, in the reported work, we describe the templating behaviour of a biomacromolecule, i.e., starch for silver nanoparticles under different conditions. The correlation of shape, size and concentration of the biomacromolecule templated silver nanoparticles with their bio-action was also investigated.

2. Materials and methods

2.1. Preparation of the silver nanoparticles

Silver nanoparticles were prepared using the reductive potential of *M. ferrea* L. aqueous leaf extract by minor modification of our previous procedure (Konwarh et al., 2010). Briefly, about 20 matured leaves of *M. ferrea* L. were washed with de-ionized water. These were blended for about 2 min and then heated in 50 mL of water for 10 min at about 60 °C. The leaf extract was filtered through a muslin cloth. In two separate reaction vessels, 200 μL of 0.1 M $AgNO_3$ (Qualigens®) was taken in 7.5 mL of 5% (w/v, g/mL) soluble starch (Qualigens®) solution, and 6 mL of the *M. ferrea* L. leaf extract, adjusted to basic pH with 0.2 M NaOH (RANKEM), was added as source of reducing agent. The first vessel was kept for aging under ambient conditions while the mixture in the second was subjected to sonication.

2.2. Statistical optimization of sonication parameters

Ultrasonication was carried out with standard sonotrode (tip-diamter 3 mm) in a high-intensity ultrasonic processor (UP200S, 24 kHz, and acoustic power density 460 W/cm^2, Hielscher Ultrasonics GmbH, Germany) in a beaker submerged in thermostatic bath at 4 °C. Response surface methodology (RSM) was used to estimate the main effect of sonication on response, i.e., the λ_{max} peak position. Three factors with three levels consisting of 32 experimental runs were used to analyze the experimental data including five replicates at the center point. This allows better estimate of the experimental error and to provide extra information in the interior of the experimental region (Haaland, 1989).

Time of sonication (C_1), cycles (C_2) and amplitude percent (C_3) were chosen as the experimental factors or the independent variables capable of influencing the λ_{max} peak position (Y). Analysis was done using coded values (−1 for C_1 = 1 min, C_2 = 0.1 and C_3 = 30%; 0 for C_1 = 3 min, C_2 = 0.5 and C_3 = 60%; 1 for C_1 = 5 min, C_2 = 0.9 and C_3 = 90%). Using this design, the experimental data were fitted according to Eq. (1) as a second order polynomial equation including individual and cross effect of each variable.

$$Y = a_0 + a_1C_1 + a_2C_1^2 + a_3C_2 + a_4C_2^2 + a_5C_3 + a_6C_3^2 + a_7C_1 \times C_2 + a_8C_1 \times C_3 + a_9C_2 \times C_3 \quad (1)$$

where a_0, a_1, a_2, a_3, a_4, a_5, a_6, a_7, a_8, a_9 are the regression coefficients. Analyses were carried out in duplicates. The data tabulated were (Table 1) the average of the measurements. Multiple regression analysis, response surface plots and statistical analyses were performed using Minitab 15 Statistical Software® (Minitab Inc., PA, USA).

After separating the matrix supported particles by centrifugal decantation, they were washed with Millipore-water to remove the excess base and unreacted silver ions.

2.3. Characterization of the starch supported silver nanoparticles

UV-spectra were analyzed in Hitachi (U-2001, Tokyo, Japan) UV spectrophotometer. FTIR spectra for the samples were recorded in a Nicolet (Impact 410, Madison, WI) FTIR spectroscopy by using KBr pellets. Size and distribution of NPs were studied using JEOL, JEM-CXII transmission electron microscope (TEM) at operating voltage of 100 kV.

2.4. Phytotoxicity analysis on C. sativus

The average germination rates of the *C. sativus* seeds (confirming to the standard of Seed Act 1966) were greater than 92% as shown by a preliminary study. Seeds were kept in a dry place in the dark under room temperature before use. These were surface sterilized in a 10% sodium hypochlorite solution for 10 min (USEPA 1996), followed by rinsing thrice with Millipore-water. They were then soaked in Millipore-water or nanoparticle suspensions for about 2 h. One piece of filter paper was put into each 100 mm × 15 mm Petri dishes, and 5 mL of the test samples (unsonicated vs. sonicated) was put into the respective Petri dishes. Seeds were then transferred onto the filter paper, with 15 seeds per dish at 1 cm or larger distance between each seed. Petri dishes were covered and sealed with tape, and placed in an incubator. After 5 days in the dark under room temperature, more than 90% of the control seeds had germinated and developed roots that were at least 18 mm long. Then, the germination was halted, seed germination rate was calculated, and seedling root length was measured. To examine which process (seed soaking or incubation after the soaking) primarily retarded the various developmental stages of the seedlings, three treatments were used: (A) both seed soaking and incubation were performed in nanoparticle suspensions; (B) seeds were soaked in nanoparticle suspensions for 2 h, and were then transferred into Petri dishes with 5 mL Millipore-water for incubation after being rinsed three times with Millipore-water; and (C) seeds were incubated in Petri dishes with 5 mL nanoparticle suspensions after being soaked in Millipore-water for 2 h. The germinated seeds were then transferred to beds prepared with sandy loam soil enriched with

Table 1
Observed and predicted values of response (λ_{max} peak position).

Time of sonication (min) (C_1)	Cycle (C_2)	Percent amplitude (C_3)	Observed response	Predicted response
−1	−1	−1	413.8	414.1
−1	−1	0	413.6	413.6
−1	−1	1	414.0	414.3
−1	0	−1	412.9	412.6
−1	0	0	412.5	412.1
−1	0	1	413.0	412.9
−1	1	−1	415.7	415.8
−1	1	0	415.4	415.4
−1	1	1	416.2	416.2
0	−1	−1	411.2	411.2
0	−1	0	411.0	410.8
0	−1	1	411.9	411.6
0	0	−1	410.0	409.6
0	0	1	410.6	410.0
0	1	−1	412.6	412.8
0	1	0	412.3	412.4
0	1	1	413.0	413.3
1	−1	−1	415.6	415.5
1	−1	0	415.4	415.2
1	−1	1	415.9	416.0
1	0	−1	413.6	413.8
1	0	0	413.2	413.5
1	0	1	414.0	414.4
1	1	−1	416.9	416.9
1	1	0	417.1	416.6
1	1	1	417.8	417.6
0	0	0	409.0	409.2
0	0	0	408.8	409.2
0	0	0	408.9	409.2
0	0	0	408.8	409.2
0	0	0	409.9	409.2

yard manure and compost. The shoot length was measured after 5 days. All studies were done in triplicates and results expressed as average of these. In conjunction to the above tests, the seeds were also soaked and incubated in the aqueous leaf extract to check any phytotoxic effect of the latter.

2.5. Effect of the nanoparticles on amplification of DNA sequence in polymerase chain reaction

The effect of silver nanoparticles on PCR was performed by employing a human 263 base pair target sequence

F: 5′-GATTAGCATACTTAGACTACTAACCTCCATG-3′
R: 5′-GATCAACTTCTGGAAAAAGCATTCCCAC-3′.

The PCR consisted of an initial denaturation at 95 °C for 1 min, followed by 32 cycles of 30 s at 95 °C, 1 min at 58 °C and 1 min at 72 °C, and a final extension of 5 min at 72 °C. The amplicons were then run on 2% agarose gels pre stained with ethidium bromide. 50 base pair molecular marker (Fermentas) was used to analyze the size of the bands. It is to be noted that the execution of this experiment was performed in accordance to the guidelines set by Tezpur University Ethical Committee.

2.6. Evaluation of anti-microbial potency of silver nanoparticles

The samples were individually tested against a panel of microorganisms including *Staphylococcus aureus* MTCC96, *Bacillus subtilis* MTCC736, *Pseudomonas aeruginosa* PN1 and *Candida albicans.* The antibacterial tests were performed as described elsewhere (Turkoglu, Duru, Mercan, Kivrak, & Gezer, 2007) after some modification. Anti-microbial activity of samples was determined by the agar-well diffusion method. All the microorganisms mentioned above were incubated (37 °C, 24 h) by inoculation into Mueller Hinton broth. *C. albicans* was incubated in Sabouraud dextrose broth (30 °C, 48 h). The culture suspensions were prepared and adjusted by comparing against 0.4–0.5 Mc Farland turbidity standard tubes. Mueller Hinton Agar and Sabouraud dextrose Agar (20 mL) were poured into each sterilized Petri dish (10 mm × 90 mm) after injecting cultures (100 μL) of bacteria and yeast and distributing medium in Petri dishes homogeneously. For the investigation of the antibacterial and anticandidal activity, the samples were filtered through a 0.22 μm membrane filter. The two prepared samples at various concentrations were introduced into the wells (6 mm) in agar plates directly. Plates injected with the yeast cultures were incubated at 30 °C for 48 h, and the bacteria were incubated at 37 °C for 24 h. At the end of the incubated period, minimum inhibitory concentration (MIC) for the respective samples was determined. Studies were performed in triplicates and with positive control of ampicillin (50 μg) for bacteria and Nystatin (10 μg) for *Candida*.

3. Results and discussion

3.1. Preparation and characterization of the starch supported 'green' branched and spherical silver nanoparticles

No absorption peak was observed in UV–visible spectrum of Ag^+ solution before addition of leaf extract, i.e., reduction, which may be attributed to Ag^+ ion's d^{10} configuration (Ulkur, Oncul, Karagoz, Yeniz, & Celikoz, 2005). After the reduction process, nucleation is followed by auto-catalytic particle growth. Myriad parameters like particle size, shape, dielectric constant of the medium and surface adsorbed species determine the position and shape of the Plasmon absorption (Zhao et al., 2008). UV–vis spectra give considerable information about the growth and shape–size accord of nanoparticles. It is pertinent to mention that the Plasmon peak and the full-width of half-maximum (fwhm) depend on the extent of colloid aggregation (Yamamoto, Fujiwara, & Watari, 2004). Colloidal aggregation resulting in larger particle size often leads to red shift in the spectrum. However, the presence of polymer in

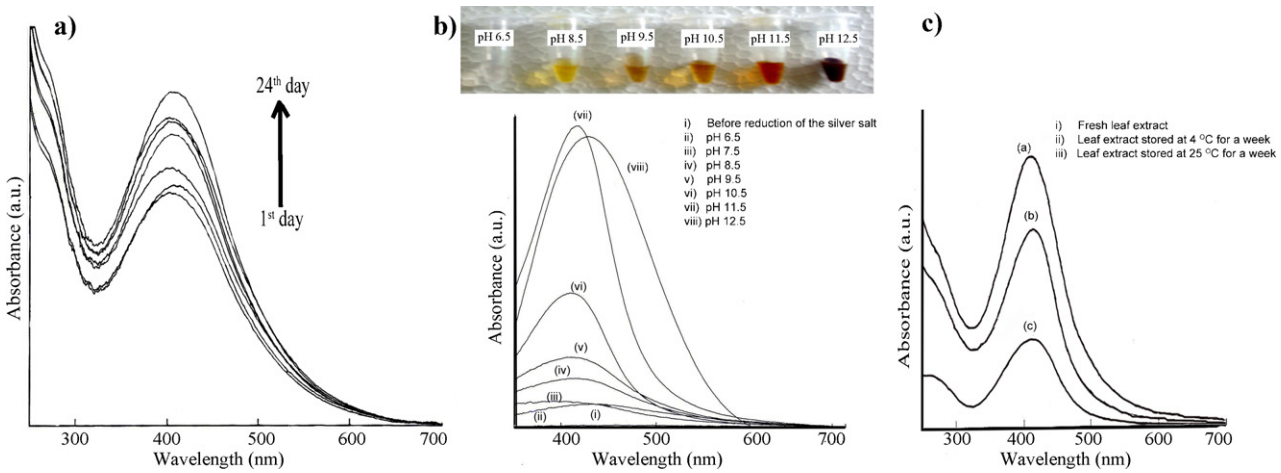

Fig. 1. UV-spectra of the starch templated silver nanoparticles (a) aged up to 24 days, (b) with variation of pH (the inset shows the colour variation of the nanosilver at different pH) and (c) on aging and storage temperature of the leaf extract.

the solution hinders the excessive nucleation and decreases the rate of growth. Recently starch stabilization of nanoparticle surfaces has been attributed to formation of nanoscopic domains with hydrophobic interior, which associates with the nanoparticle surface, while the amylose hydrophilic surface is expected to confer solubility and steric stabilization (Singh, Sinha, Premkumar, Singh, & Mandal, 2010).

The influence of pH could be directly visualized via the gradual colour change from almost transparent at pH 6.0 to light yellow at pH 8.0 and finally to deep brown at pH 13 (Fig. 1b inset). In acidic pH, the association among the active compounds of the leaf extract through H-bonding is expected to be more pronounced which stabilize the structures and as a result of which these compounds are not effectively utilized in reduction process. This feature is reversed with increase in basicity. With the increase of pH up to 11.5, the intensity of the peak at 410 nm kept on increasing which indicates the progressive generation of the nanoparticles. However, further increase in the basicity of the medium resulted in a red shift of the peak position towards 430 nm, indicative of larger particle size due to overgrowth. It is important to note that very high alkaline condition of the medium may lead to weakening of the association (H-bonding) even for the starch matrix and thereby diminishing its templating potential to support small sized nanoparticles. This may explain the red-shift for the nanoparticles formed above pH 11.5. Authors would like to mention that the samples prepared at pH 11.5 have been used for various analyses described underneath.

It was also interesting to note the decrease in intensity of the peak at 410 nm for the samples prepared corresponding to the progressive aging of the leaf extract used for reduction (Fig. 1c). The fresh extract gave the highest peak followed by that stored in the refrigerator at 4 °C and the least intense peak was observed for the extract stored at room temperature (ca. 25 °C). The influence of aging of the leaf extract may be bracketed together with the likely progressive aerial oxidation of the active reducing components of the leaf extract, manifested via a dip in the SPR peak intensity of the generated silver nanoparticles. Nevertheless, the branched structure was generated through a simple aging process. Next, we turned to optimize the sonication parameters for generating matrix supported silver nanoparticles stabilized within a narrow size domain without coalescing.

It is important to mention that no characteristic silver's SPR peak was observed when starch alone was used at ambient conditions without the input of external thermal energy. This additional energy is required for the breakdown of starch to generate active –OH groups through release of glucose units for the reduction. However, the monovalent silver ion is primarily reduced by –OH group of the active components of the leaf extract, which is oxidized to corresponding carbonyl group, as indicated by the IR spectra (Fig. 2).

The distribution of 72 h aged starch assisted silver nanoparticles within a size window of (1–24 nm) and average particle size of 8.75 nm (Fig. 3a) was indicative of non-coherent nucleation—a probable outcome of an interfacial mechanism of the reduction process. During non-coherent or heterogeneous nucleation, the time dependence of the transformation rate is determined by the relative magnitudes of the nucleation and growth rates. The formation and growth of Ag nanoparticles was not completed even after 72 h of aging. A progressive increase in the intensity of the Surface Plasmon Resonance (SPR) band at around 400–420 nm with aging time till 24 days could be seen (Fig. 1a). Aging for about 24 days showed the formation of nanobranches with diameter 11.5 nm, generating a branched structure with 440 nm length along the long axis (Fig. 3b). In our system, we have seen that there is an interaction of the leaf extract components and starch matrix as evident from the FTIR spectra, indicated by the broadening of the band at around 3600–3200 cm^{-1} (Fig. 2). As such this complex structure may now act as the morphology-directing agent, promoted together by gradual nucleation. With greater passage of aging period (in the absence of any external agitation of the system), the interaction with the *M. ferrea* leaf extract components and the helical conformation and templating effect of starch might direct the growth of nanobranches emanating from the central nanoparticle core, thereby generating the branched structure.

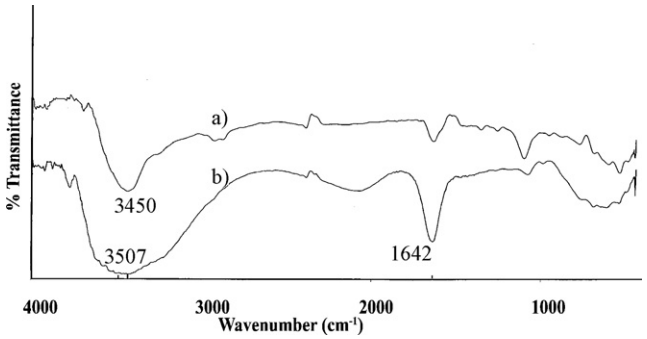

Fig. 2. FTIR spectra of (a) *M. ferrea* L. aqueous leaf extract and (b) *M. ferrea* L. leaf extract and starch mixture after reduction of metallic silver.

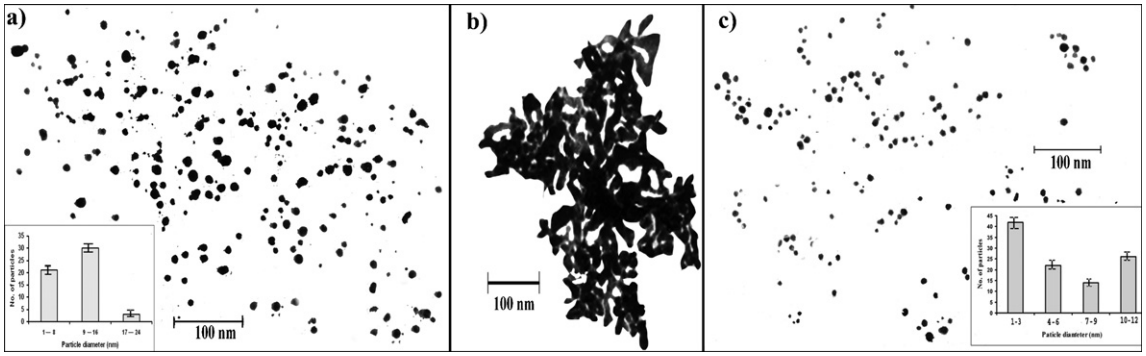

Fig. 3. TEM image of starch templated silver nanoparticles obtained (a) upon aging for 72 h (the inset shows the histogram of the particle size distribution), (b) upon aging for 24 days (branched silver nanostructure) and (c) under statistically optimized sonication parameters (the inset shows the histogram of the particle size distribution).

TEM images of the colloidal samples were recorded after evaporation of the solvent resulting in the non-extended conformation of the polymer. This might have also facilitated a greater aggregation. It is to be noted that the UV–vis spectra of the system subjected to aging, as recorded in Fig. 1, is resulting from the solution phase or finely dispersed phase of the sample. The branched structure was most probably absent in the sample used for recording the UV–vis spectra as its presence was expected to exhibit considerable red shift.

It is established that the atoms in nanostructured metals tend to relax towards minimum free energy content from the grain boundaries and grain boundary joints. In these interfacial regions, orientational transitions, non-equilibrium atomic densities and coordination numbers reside (Bicelli, Bozzini, Mele, & D'Urzo, 2008). The inter-crystalline volume represents a region of stored excess energy with respect to the bulk of a grain. The structure of grain joints is unstable even at ambient temperature and tends to evolve towards a more ordered state, affecting the density of crystalline defects, grain size, crystallographic orientation and grain boundary structure. Under annealing, the nanosized crystallites may even start to grow in a random manner, some of them act as nuclei and preferentially start to grow at the expense of the surrounding nanocrystalline material. Thus the present study leaves scope for the material scientists to delve into and validate these probabilities for the carbohydrate templated 'green' silver nanoparticles.

The separation or combination between two particles, exhibiting constant Brownian motion in a continuous solution is governed by the inter-particular net repulsive or attractive energies as well the nature of interfacial zone To produce good silver particle dispersion in a solution, a change in the inter-particle interfacial region by either chemical or physical methods is necessary. We switched to analyze and statistically optimize the effect of sonication, a physical strategy, on directing the shape–size parameters of the prepared nanoparticles. The influence of sonication with three variable parameters, namely, duration of sonication (min), cycle and percent amplitude on the shift of λ_{max} position in the UV–vis spectra of the samples was analyzed statistically using RSM.

The parameters of Eq. (1), given in the experimental section were determined by multiple regression analysis. The overall second-order polynomial equation is represented as

$$Y = 409.2 + 0.689C_1 + 3.6C_1^2 + 0.811C_2 + 2.4C_2^2 + 0.228C_3 + 0.617C_3^2 - 0.083C_1 \times C_2 + 0.067C_1 \times C_3 + 0.05C_2 \times C_3$$

All the three chosen variables exerted both linear and quadratic effect on the λ_{max} position of the sample analyzed

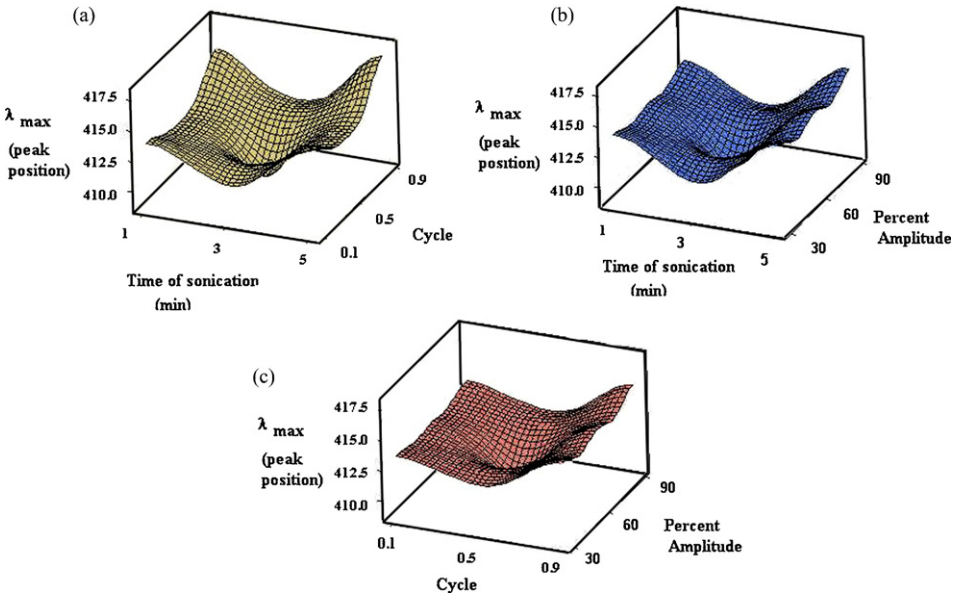

Fig. 4. Response surface plots showing λ_{max} position versus (a) time of sonication versus cycles, (b) time of sonication versus percent amplitude and (c) cycles versus percent amplitude.

Table 2
Model coefficients estimated by multiple regressions (model adequacy checking).

Factor	Coefficient	*t*-Value	*p*-Value
Constant	409.2	3450.79	0.000 < 0.05
C_1	0.689	8.282	0.000 < 0.05
C_2	0.811	9.751	0.000 < 0.05
C_3	0.228	2.738	0.012 < 0.05
$C_1 \times C_1$	3.6	27.284	0.000 < 0.05
$C_2 \times C_2$	2.4	18.189	0.000 < 0.05
$C_3 \times C_3$	0.617	4.674	0.000 < 0.05
$C_1 \times C_2$	−0.083	−0.818	0.422 > 0.05
$C_1 \times C_3$	0.067	0.654	0.520 > 0.05
$C_2 \times C_3$	0.05	0.491	0.628 > 0.05

(Fig. 4). The model contained three two-way interactions (time of sonication × cycles, time of sonication × percent amplitude and cycles × percent amplitude). For each of these interactions, *p*-value was more than 0.05 (chosen α value) (Table 2) and as such these cross-interactions did not have a significant effect on determining the λ_{max} position. The model yielded a R^2 value that could explain up to 98.76% of the sample variance, indicating a good fit of the data with the devised model. Minimum particle size is expected with the data set of 3 min of sonication, 0.5 cycle and 60% amplitude. Fig. 3c shows the spherical shaped silver nanoparticles homogenously distributed within a size window of 1–12 nm, with average diameter 5.4 nm, obtained under optimized sonication parameters with maximum number of particles between 1 and 3 nm.

Sonication is a common strategy to obtain well dispersed nanoparticles within a narrow size window. However, it is critical to control the timing and amplitude. Too much energy input in the system can lead to increased inter-particular collision, resulting in formation of larger agglomerates and consequent red shift in the UV–vis spectrum. On the other hand, the aid for dispersion may be limited if optimal energy is not supplied to the system. Response surface methodology helped in optimizing the sonication parameters to obtain narrow-sized particles, correlated with observed blue shift. The choice of a second order polynomial regression model was satisfactory, and the estimation of coefficients by multiple linear regressions was a priori much more explanatory than that obtained by any classical analysis of variance.

It was interesting to note the stability of the system even for the samples analyzed after 4 months of preparation and storage at room temperature (image not shown) as indicated by the retention of the peak sharpness and position at 408 nm with almost no red shift (confirmed by TEM imaging, not shown here).

The premonition of a differential shape–size influence of the prepared starch assisted silver nanoparticles on the bio-action prompted us to test the phytotoxicity, anti-microbial action and the consequence of incubation of the samples with mammalian DNA sequence in PCR.

3.2. Evaluation of phytotoxicity on C. sativus

In our study, seeds showing emergence of radicle or cotyledon coming out of the seed coat were recorded as being germinated. Prior to membrane invagination in plant cells, exotics penetrate through the semi-permeable cell wall, primarily composed of polymeric carbohydrates with pore size less than several nanometers (Carpita, Sabularse, Montezinos, & Delmer, 1979). We were inerested to check if such possible penetration of the silver nanoparticles could modulate the phyto-physiology. From the phytotoxicity assessment, it could be inferred that minor variations do exist in the interaction and penetration of the samples through the seed coat. We believe that the size and shape factors of the samples affect the average germination rate of the seeds. As could be seen from Table 3, the sonicated sample decelerates the average germination rate as compared to that for the unsonicated sample. Interestingly, the three treatments we had devised did show minor variations. Treatment B for both the samples showed germination rate parallel to that of the control (without any treatment). However, treatments A and C inhibited the germination rate to greater extent and in particular for the sonicated sample. In order to further validate whether the process of soaking or incubation led to inhibition, we increased the soaking time from 2 to 8 h and found almost similar rate of inhibition. Thus, the incubation parameters seemed to be more critical than soaking conditions in deciding the phytotoxicity profile of the nanomaterials.

The differential effect on the seed germination may be attributed to smaller size and spherical shape of the Ag NPs in the sonicated sample that could be mobilized into the plant cells with greater ease as compared to the branched structure. Roots being the initial targets to confront with excess concentrations of pollutants, toxic symptoms seem to appear more in roots rather than in shoots (Sresty & Rao, 1999). Radicles, after penetrating the seed coats, could contact the nanoparticles directly. The tested samples did not show statistically significant variations in the root elongation. However, probably more internalization of the sonicated Ag NPs did affect the radicle length to a greater extent in comparison to the unsonicated sample. Similar trend was noted for shoot-length elongation. However, no significant variations were noted for the survival percentage of the seedlings post-transplantation. It is to be noted that the aqueous leaf extract did not influence the seed-germination and the growth of the cucumber seedlings post transplantation.

However, certain questions still remain unanswered. Will the effect of the prepared samples and the consequences of the internalization and bio-distribution be same for both dicot and monocot plants? Does the penetration of Ag NPs into the root cells help the plants to ward off soil pathogens or lead to the loss of beneficial microflora peripheral to the roots? Furthermore, more research is needed to clarify the contribution of dissolution to the toxicity of metal-based nanoparticles.

3.3. Concentration dependent compromise on replication of mammalian DNA sequence in PCR

The preliminary genotoxicity test of the prepared nanosilver, assessed through effect on PCR amplification showed a concentration dependent inhibition. Silver (Basu, Jana, Pande, & Pal, 2008; Hatchert & White, 1996) tends to have a high affinity for phosphorous- and sulphur-containing compounds such as DNA. As compared to the branched structure, the smaller sized particles in the sonicated sample with greater surface area may bind more efficiently with the DNA and as such interference with the replication machinery may be more profound than the former. This plausibility may be even complemented by their probable interaction with the polymerase enzyme. These need further insight and detailed *in vivo* studies. Nevertheless, this preliminary study does unveil the potential of the nanoparticles to become a risk factor especially when used at higher concentrations. Further tests into the effect of the silver nanoparticle on humans are important.

In the presence of silver nanoparticles up to a concentration of 14 nM, we observed that there was no inhibition (for both the samples) of the PCR amplification when compared to the control band (Fig. 5a). The concentration of both the samples when increased to 50 μM showed complete inhibition (image not shown). Therefore, we decreased the concentration further and observed (Fig. 5b) that at 3.5 and 7 μM concentration of the nanoparticles for the unsonicated sample, the amplification was significantly less (R_1 and R_2) than the control (C) (without treatment with the silver nanoparticles) with no amplification at 14 μM (R_3). However, the same concentrations for the sonicated sample were completely

Table 3
Phytotoxicity assessment of the prepared nanomaterials—ramified/unsonicated (R) and sonicated (S) silver nanoparticles on germination and growth of *Cucumis sativus*.

Process (for details, please refer to the text)	In the laboratory conditions				In field conditions			
	Average germination rate (%) of the seeds		Average radicle length (mm) after 5 days incubation		Average survival rate (%) of seedlings 5 days post-transplantation		Average shoot length (cm) 5 days post-germination	
	R	S	R	S	R	S	R	S
A	94	87	18	16	100	100	14	13
B	97	96	20	19	100	100	15	13.5
C	95	89	18	17	100	100	14	12.5

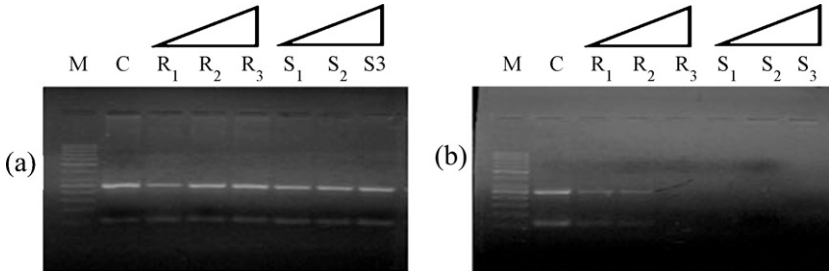

Fig. 5. Gel electrophoresis of PCR amplified products. M, marker; C, control (untreated DNA); lanes (R_1, R_2 and R_3) and (S_1, S_2 and S_3), samples treated with (a) 3.5, 7, 14 nM and (b) 3.5, 7, 14 μM of branched and spherical silver nanoparticles respectively.

inhibitory for the amplifications (S_1, S_2 and S_3) (Fig. 5b). As far as the aqueous leaf extract is concerned, no inhibitory action was noted in the PCR (figure not shown).

3.4. Differential anti-microbial potency

The prepared samples exhibited anti-microbial activity against a panel of test-organisms. A number of interesting results emanated from the experiment. The anti-microbial action was more pronounced against Gram positive bacteria (*S. aureus* and *B. subtilis*) than Gram negative bacteria (*P. aeruginosa*). The samples showed anti-candidal activity as well. The MIC of the sonicated sample (6.32, 6.32, 25.3 and 12.65 μg/mL) was less as compared to the unsonicated sample (12.65, 25.3, 37.95 and 32.5 μg/mL) against *S. aureus*, *B. subtilis*, *P. aeruginosa* and *C. albicans* resepectively. Various mechanisms (Sharma et al., 2009) have been propounded for the anti-microbial action of Ag NPs. These include, setting the cell membrane permeability out of gear primarily by immediate dissipation of the proton motive force and interaction with sulphur and phosphorus containing macromolecules like DNA and thereby affecting the replication machinery.

The smaller particles in the sonicated sample with larger surface area not only might interact with the membrane surface but are likely to be more penetrating than the larger branched structure. Considering the surface area of prepared silver nanostructures, it is expected that if alteration of the membrane permeability is the main route of anti-microbial action, the spherical particles should be multi-times potent than the branched structure. The MIC values of the sonicated sample should be significantly less when compared to that of the branched structure. The MIC data shows that the shape of the nanoparticles has a critical role to play. In the branched structure, the geometry helps in confining of the microorganisms for a longer duration than the mobile spherical particles. Furthermore, anti-microbial action was more pronounced against Gram positive bacteria than Gram negative bacteria. This may be due to the differential interaction of the Ag NPs with the molecular moieties at the surface of the two groups of the bacterial species and probably the overall different cell-wall architecture influences the anti-bacterial action. The above results shore up the inclusion of these silver nanoparticles in various materials like paints and industrial coatings. However, further toxicity assessment of these prepared samples is a must.

4. Conclusion

In this present work we have reported about the morphology-directing action of starch-*M. ferrea* L. aqueous leaf extract complex to generate branched nanostructure, obtained on aging. On the other hand well dispersed silver nanoparticles (obtained upon statistical optimization of sonication parameters) hold promise for multitude of application-oriented utilities. The shape–size–concentration accord of the prepared starch templated silver nanoparticles was echoed by the differential effect on various biosystems (*C. sativus*, mammalian DNA and bacterial and fungal species). The reported system supports the switching over to bioresources (viz., starch and bioreductant in this case) for achieving easy and inexpensive shape–size tuning of nanoparticles. However, the results show that mere switching to greener route may not be the dead end but calls for compilation of comprehensive toxicity profile.

Acknowledgements

Mr. Rocktotpal Konwarh sincerely acknowledges the receipt of his Junior Research Fellowship from the Department of Biotechnology, New Delhi. RSIC, NEHU, Shillong is thankfully acknowledged for the TEM imaging.

References

Babu, V. R., Kim, C., Kim, S., Ahn, C., & Lee, Y.-I. (2010). Development of semi-interpenetrating carbohydrate polymeric hydrogels embedded silver nanoparticles and its facile studies on *E. coli*. *Carbohydrate Polymers*, *81*(2), 196–202.

Basu, S., Jana, S., Pande, S., & Pal, T. J. (2008). Interaction of DNA bases with silver nanoparticles: Assembly quantified through SPRS and SERS. *Journal of Colloid and Interface Science*, *321*, 288–293.

Bicelli, L. P., Bozzini, B., Mele, C., & D'Urzo, L. (2008). A review of nanostrucutral aspects of metal electrodeposition. *International Journal of Electrochemical Science*, *3*, 356–408.

Bourgeat-Lami, E., & Lang, J. J. (1998). Encapsulation of inorganic particles by dispersion polymerization in polar media 1. Silica nanoparticles encapsulated by polystyrene. *Journal of Colloid and Interface Science*, *197*, 293–308.

Bozanic, D. K., Djokovic, V., Blanusa, J., Nair, P. S., Georges, M. K., & Radhakrishnan, T. (2007). Preparation and properties of nano-sized Ag and Ag_2S particles in biopolymer matrix. *European Physical Journal E: Soft Matter and Biological Physics*, *22*, 51.

Carpita, N., Sabularse, D., Montezinos, D., & Delmer, D. P. (1979). Determination of the pore size of cell walls of living plant cells. *Science*, *205*, 1144–1147.

Govindachari, T. R., Viswanathan, N., Pai, B. R., Rao, R., & Srinivasan, M. (1967). Triterpenes of *calophyllum inophyllum* linn. *Tetrahedron*, *23*(4), 1901–1910.

Haaland, P. D. (1989). Statistical problem solving. In P. D. Haaland (Ed.), *Experimental design in biotechnology* (pp. 1–18). New York: Marcel Dekker, Inc.

Hatchert, D. W., & White, H. S. (1996). Electrochemistry of sulfur adlayers on the low index faces of silver. *The Journal of Physical Chemistry*, *100*, 9854–9859.

Jackson, J. B., & Halas, N. J. (2001). Silver nanoshells: Variations in morphologies and optical properties. *The Journal of Physical Chemistry B*, *105*, 2743–2746.

Konwarh, R., Kalita, D., Mahanta, C. L., Mandal, M., & Karak, N. (2010). Magnetically recyclable, antimicrobial, and catalytically enhanced polymer-assisted "green" nanosystem-immobilized *Aspergillus niger* amyloglucosidase. *Applied Microbiology and Biotechnology*, doi:10.1007/s00253-010r-r2658-4

Korbekandi, H., Iravani, S., & Abbasi, S. (2009). Production of nanoparticles using organisms. *Critical Reviews in Biotechnology*, *29*(4), 279–306.

Lin, D., & Xing, B. (2008). Root uptake and phytotoxicity of ZnO nanoparticles. *Environmental Science & Technology*, *42*(15), 5580–5585.

Lu, Q., Gao, F., & Komarneni, S. (2005). A green chemical approach to the synthesis of tellurium nanowires. *Langmuir*, *21*, 6002–6005.

Sharma, V. K., Yngard, R. A., & Lin, Y. (2009). Silver nanoparticles: Green synthesis and their antimicrobial activities. *Advances in Colloid and Interface Science*, *145*, 83–96.

Singh, M., Sinha, I., & Mandal, R. K. (2009). Role of pH in the green synthesis of silver nanoparticles. *Materials Letter*, *63*, 425–427.

Singh, M., Sinha, I., Premkumar, M., Singh, A. K., & Mandal, R. K. (2010). Structural and surface plasmon behavior of Cu nanoparticles using different stabilizers. *Colloids Surface A: Physicochemical and Engineering Aspects*, *359*, 88–94. doi:10.1016/j.colsurfa. 2010.01.069

Singh, M., Sinha, I., Singh, A. K., & Mandal, R. K. (2010). Formation of fractal aggregates during green synthesis of silver nanoparticles. *Journal of Nanoparticle Research*, doi:10.1007/s11051-010r-r0001-8

Sresty, T. V. S., & Rao, K. V. M. (1999). Ultrastructural alterations in response to zinc and nickel stress in the root cells of pigeonpea. *Environmental and Experimental Botany*, *41*, 3–13.

Turkoglu, A., Duru, E. M., Mercan, N., Kivrak, I., & Gezer, K. (2007). Antioxidant and antimicrobial activities of *Laetiporus sulphureus* (Bull.) Murrill. *Food Chemistry*, *101*, 267–273.

Ulkur, E., Oncul, O., Karagoz, H., Yeniz, E., & Celikoz, B. (2005). Comparison of silver-coated dressing (acticoat), chlorhexidine acetate 0.5% (bactigras), and fusidic acid 2% (fucidin) for topical antibacterial effect in methicillin-resistant Staphylococci-contaminated, full-skin thickness rat burn wounds. *Burns*, *31*, 874–877.

Vigneshwaran, N., Nachane, R. P., Balasubramanya, R. H., & Varadarajan, P. V. (2006). A novel one-pot 'green' synthesis of stable silver nanoparticles using soluble starch. *Carbohydrate Research*, *341*, 2012–2018.

Yamamoto, S., Fujiwara, K., & Watari, H. (2004). Surface-enhanced Raman scattering from oleate-stabilized silver colloids at a liquid/liquid interface. *Analytical Sciences*, *20*, 1347–1352.

Yang, F., Hong, F. S., You, W. J., Liu, C., Gao, F. Q., Wu, C., et al. (2006). Influences of nano-anatase TiO_2 on the nitrogen metabolism of growing spinach. *Biological Trace Element Research*, *110*, 179–190.

Yang, W., Shen, C., Ji, Q., An, H., Wang, J., Liu, Q., et al. (2009). Food storage material silver nanoparticles interfere with DNA replication fidelity and bind with DNA. *Nanotechnology*, *20*, 085102.

Zhao, J., Pinchuk, A. O., Mcmahon, J. M., Li, S., Ausman, L. K., Atkinson, A. L., et al. (2008). Methods for describing the electromagnetic properties of silver and gold nanoparticles. *Accounts of Chemical Research*, *41*(12), 1710–1720.

Ziolo, R. F., Giannelis, E. P., Weinstein, B. A., O'Horo, M. P., Ganguly, B. N., Mehrotra, V., et al. (1992). Matrix-mediated synthesis of nanocrystalline ggr-Fe_2O_3: A new optically transparent magnetic material. *Science*, *257*, 219–223.